RESEARCH ARTICLE

Beamforming Network Based on Novel Continuously Tunable Couplers

**VITALY KIRILLOV[1], (Student Member, IEEE), DMITRY KOZLOV[2],
PAWEL RULIKOWSKI[3], (Member, IEEE), AND SENAD BULJA[4], (Senior Member, IEEE)**

[1]Centre for Wireless Innovation (CWI), Institute of Electronics Communications and Information Technology, Queen's University Belfast, Belfast BT7 1NN, U.K.
[2]DPD and PA Department, Nokia Technology Center, 89081 Ulm, Germany
[3]Former Nokia Bell Labs, RF Research, Dublin, D08 AH31 Ireland
[4]Wireless Communications Laboratory, Tyndall National Institute, Dublin, D08 WV88 Ireland

Corresponding author: Dmitry Kozlov (dmitry.1.kozlov@nokia.com)

ABSTRACT In this paper a new beamforming network for a given number of antenna elements is presented. The new architecture is capable of adaptively distributing an input RF signal among all individual antenna elements with an arbitrary selection of magnitudes and phases. The presented architecture is based on a novel coupler design, which is theoretically capable of an arbitrary division of power between its two output ports. The control of power division ratio is achieved by means of active elements capable of modulating its reactance, such as varactor diodes. As a demonstrator of the proposed beamforming concept, a feeder network for an array of 16 antenna elements is designed, simulated and fabricated to operate at a frequency of 2.5 GHz. The obtained results indicate an unprecedented level of reconfigurability, showing that the input signal can be divided among the antenna elements with arbitrary values of magnitudes and phases. The results are discussed.

INDEX TERMS Beamforming networks, 5G, reconfigurable circuits, coupler.
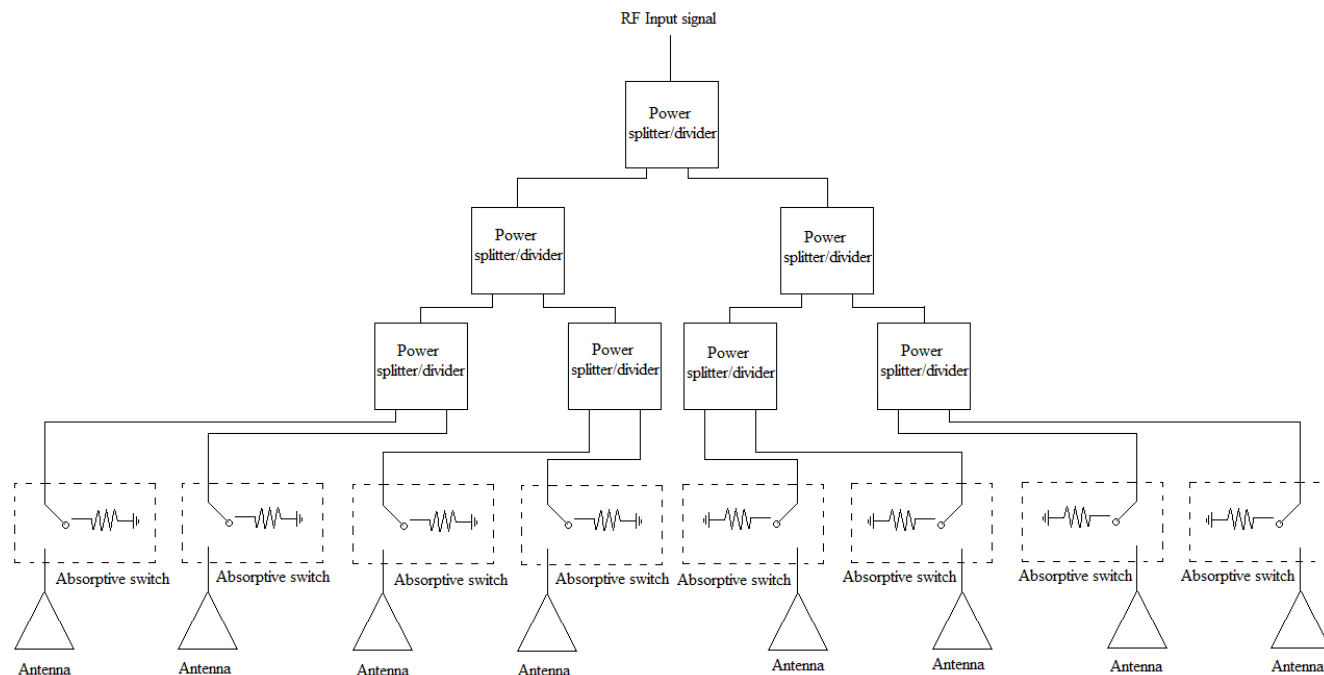
I. INTRODUCTION

Flexible spectrum usage and hardware reconfigurability are among the key aspects of future communications systems, such as advanced 5G and the forthcoming 6G technologies [1]. Such hardware flexibility is expected to cater for the enablement of networks capable of low end-to-end latency, high data rates and network adaptability. Viewed through the RF/mm-wave front-end point of view, flexible access to the network is expected to manifest itself not only through frequency reconfigurability, where communication systems will be able to modify the frequency of operation of its transceiver (TRX) architectures, but also its radiation characteristics, exemplary represented though antenna gain and beamwidth, to name but a couple. Here, beam-steering capabilities of the RF/mm-wave front ends are of utmost importance.

Beam-steering is usually enabled through the use of antenna arrays [2], [3], where specific and pre-determined

magnitude and phase weights are applied to each antenna elements in order to obtain desired radiation characteristics (beam-steering). Alternative methods for beam-steering also exist, such as the ones relying on antenna lenses (Luneburg lens, for example), [3], [4]. In this case, beam-steering is achieved by feeding the lens structure at distinct positions on the surface of the lens. The dimensions of the lens antenna dictate the achievable gain and, usually, its main feature size is of the order of several wavelengths, rendering the lens physically large for lower frequencies (below 6 GHz).

In standard beam-steering applications deploying antenna arrays, the number of antenna elements dictates the achievable gain through the array factor and the radiation characteristics of the individual antenna. In general, the greater the number of antenna elements, the greater the gain and the narrower the beamwidth [5]. Narrow beamwidths are beneficial from the point of view of point-to-point communications, resulting in high Signal-to-Noise Ratios (SNR), however, there exist instances where the gain and, hence, the beamwidth of the array needs to be flexible and tailored to the specific communication scenario. Instances for this are

The associate editor coordinating the review of this manuscript and approving it for publication was Bilal Khawaja.

FIGURE 1. An array of eight switched antenna elements (phase shifters preceding antennas are omitted for brevity).

many – periodically, the antenna arrays may be tasked to perform broadcast communications, aimed to address many users at once or, in another example, the number of active antennas to be used in a certain scenario will be lower than those provided in the array, in order to enable the array to provide a wider coverage. In such cases, the antenna array needs to be able to switch off the not-needed antenna elements either through the use of some kind of absorptive switches or resort to the use of flexible power dividers capable of directing RF power the desired antenna elements. The use of absorptive switches deployed immediately before the antenna element, Fig. 1, appears to be an optimum approach, however, it comes at expense of wasting the valuable RF power as heat in the absorptive switches. In this case fixed power splitters/dividers are widely used [6]. The second approach, centred on the capability of power dividers to arbitrarily direct RF power to the desired antenna element(s) appears to be an optimum choice, however, there exists a lack of suitable power dividers in the literature. For example, in [7], an interesting magnitude and phase reconfigurable power distribution based on power dividers and phase shifters was presented. Even though such approaches offer reasonable results, the network is cumbersome. In another example, [8] a Wilkinson variable power divider capable of adjusting the power dividing ratio from 2.59 to 10.4 was presented. Even though the divider ratio may be suitable for a variety of applications, the fact that the return loss is a function of power division is a serious limitation. In a similar manner, in [9], [10] a switched-path 3-way power divider is presented and is capable of directing input power to any of the 3 desired output ports, however, the

power division ratio is not reconfigurable. As another example, a coupled microstrip lines splitter was presented in [11], [12], where the reconfigurability aspect was provided by the addition of varactor diodes connected at the centre points of microstrip lines. Such a simple structure is capable of yielding a power ratio of about 2.4, however, it had the drawback of having the return loss dependent on the power division ratio. An interesting configuration of the power divider is presented in [13], [14], which showed the use of a varactor diode in the modified circuitry of a rat-race coupler to yield power ratios of about 15 dB. Even though such a ratio is high enough to accommodate a wide array of applications, scenarios exist where even higher dynamic ratios are needed. An interesting configuration of a variable split power divider was presented in [15], which consisted of two 3-dB couplers connected back-to-back through a shunted varactor diode. The paper presented that the extent of variable power split between two ports is possible and that it is dependent on the reactance values of the varactor diodes.

The goal of the present paper lies in the provision of the new topology of variable couplers, capable of providing arbitrary power splits as a function of an external stimulus in an efficient way and without wasting RF power unnecessarily. Such a coupler builds upon the concepts of [14] and [15] and provides exact circuit topologies capable to fully switch ON and OFF desired signal paths. The performance of the proposed coupler is not only assessed in the standalone configuration, but also in the reconfigurable beamforming network of an antenna array. The fabricated novel couplers and the corresponding beam-reconfigurable array are made to
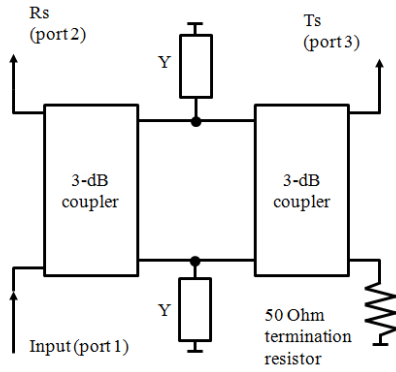
FIGURE 2. Proposed continuously variable coupler.

FIGURE 3. Circuits capable of providing admittance variation as C_v increases; $\infty \to 0$ (a) $0 \to \infty$ (b) and from $\infty \to 0 \to \infty$ (c). Biasing circuit omitted for brevity.

operate at a frequency of 2.5 GHz. This frequency was chosen due to a relatively simple implementation of the proposed beamforming network based on Printed Circuit Board (PCB) technology and the commercial availability of surface mount components, such as inductors and capacitors. Implementations at higher frequencies would likely involve the realisations of lumped elements in a distributed form due to lower commercial availability and, also, in order to reduce the losses of the circuit.

II. THEORY OF OPERATION OF NOVEL COUPLER

The proposed coupler is presented in Fig. 2. As mentioned earlier, it consists of two 3-dB couplers connected back-to-back through a shunted variable admittance, Y. The even- and odd- mode analysis performed on the power splitter infers the following S-parameters matrix:

$$[S] = \begin{pmatrix} 0 & 0 & S_{13} & S_{14} \\ 0 & 0 & S_{23} & S_{24} \\ S_{31} & S_{32} & 0 & 0 \\ S_{41} & S_{42} & 0 & 0 \end{pmatrix} \quad (1)$$

where

$$S_{13} = S_{24} = S_{31} = S_{42} = T_s = \frac{j2}{2 + Z_0 Y} \quad (2)$$

$$S_{14} = S_{23} = S_{32} = S_{41} = R_s = -\frac{jZ_0 Y}{2 + Z_0 Y} \quad (3)$$

where, T_s and R_s represent the transmission and reflection coefficients and Z_0 is the characteristic impedance. Further, provided that admittance Y is purely imaginary, the differential phase between the transmission and reflection coefficients is always 90° and the power conservation criterion is unconditionally satisfied, i.e.

$$\sum_{n=1}^{n} S_{ni} \cdot S_{ni}^* = 1 \quad (4)$$

In other words, no power is delivered to the isolation port, represented by resistor R_t. The two ultimate cases for the reflected and transmitted signals are when admittance Y is allowed to be either 0 or ∞.
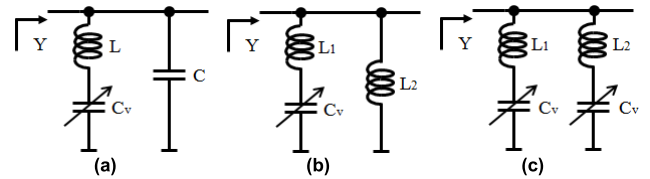
For the case when $Y = 0$ the transmitted and reflected signals become:

$$T_s (Y = 0) = j \text{ and } R_s (Y = 0) = 0 \quad (5)$$

And for the case when $Y \to \infty$

$$T_s (Y \to \infty) = 0 \text{ and } R_s (Y \to \infty) = -j \quad (6)$$

(5) and (6) infer that in order to obtain a capability to fully switch ON and OFF one of the arms of the proposed variable coupler, admittance Y needs to be able attain arbitrary values ranging from 0 to ∞.

The circuits capable of providing such admittance values as a function of a variable capacitance are shown in Fig. 3. With respect to the circuit of Fig. 3 (a), the values of the inductor, L, and capacitor, C, are determined in the following fashion:

$$L = \frac{1}{\omega^2 C_{vmin}} \quad \text{and} \quad C = \frac{C_{vmin} C_{vmax}}{C_{vmax} - C_{vmin}} \quad (7)$$

Similarly, the values of the discrete components, L_1 and L_2 for the circuit of Fig. 3 (b) are obtained using the following equations:

$$L_1 = \frac{1}{\omega^2 C_{vmax}} \quad \text{and} \quad L_2 = \frac{C_{vmax} - C_{vmin}}{\omega^2 C_{vmax} C_{vmin}} \quad (8)$$

Lastly, the values of L_1 and L_2 for the circuit of Fig. 3 (c) are obtained using:

$$L_1 = \frac{1}{\omega^2 C_{vmax}} \quad \text{and} \quad L_2 = \frac{1}{\omega^2 C_{vmin}} \quad (9)$$

Choosing a particular configuration is dependent on many parameters, such as the slope of the admittance, $\left(\frac{dY}{d\omega}\right)$ which will dictate the pertinent bandwidth of operation, ease of implementation and practical considerations. In terms of practical considerations, the circuit of Fig. 3 (c) is the optimum approach, as the boundaries at which $Y \to \infty$ are made to occur at both C_{vmin} and C_{vmax}, therefore ensuring the correct operation even in the case of manufacturing uncertainties of the active device.

As a demonstrator, a variable coupler was designed to operate at a frequency of 2.5 GHz. Its schematic is shown on Fig. 4. The divider contains two 3-dB 90° hybrid couplers from Anaren with a part number (X3C25F1-03S) [17], connected in cascade through two series resonant circuits in the direct and coupled arms, respectively. The direct port of the second coupler is connected to a termination resistor. To obtain the highest possible power division ratio, the
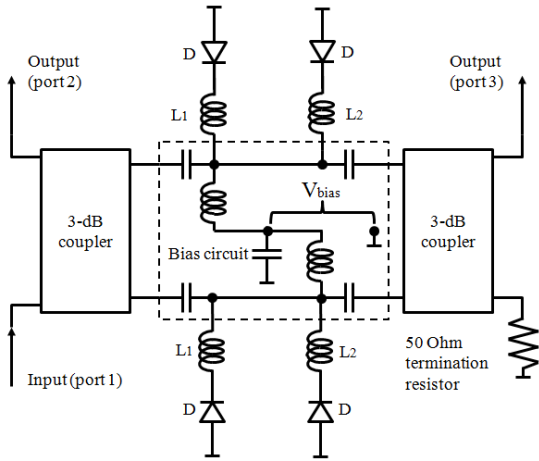
FIGURE 4. Equivalent circuit of the coupler.

electrical circuit of Fig. 3 (c) was chosen as the resonant circuit. For the active device, a hyperabrupt varactor diode from Macom (MAVR-000202) [18] was used in this work.

This varactor diode exhibits a capacitance variation of the bare die between 0.6 pF (DC bias voltage of 20 V) to 2.7 pF (DC bias of 4 V), which is typical for hyperabrupt junction diodes. However, in the present application we are limited to the maximum DC bias voltage of 13 V. This is due to the fact that the DC bias voltage is sourced from the Digital-to-Analog-Converter (DAC) AD5371 from Analog Devices [19], which is limited to a maximum 13 V output. This infers that the minimum capacitance of 0.6 pF, as stated in the diode's datasheet obtained at 20 V, is not achievable with this set-up. The capacitance of the varactor diode at 13 V was experimentally determined to be equal to 0.72 pF. Due to the reduction in the maximum DC bias voltage applicable to the diode and in order to increase the DC bias voltage range used to control to the characteristics of the present coupler and, hence, reduce the losses, it was decided to use the diode's capacitance achievable at 2V, instead of 4V, which is specified in the diode's datasheet. However, since the capacitance of the varactor diode at 2V is not specified in the datasheet, it was experimentally determined to be 4 pF. Using (9) in conjunction with the given capacitor values (0.72 pF and 4 pF), the values of the inductors (E series), [20] are obtained:

$$L_1 = 1\text{nH and } L_2 = 3.9\text{nH}$$

Taking into account the inductance effects of the PCB mounting pads, the values for the inductors L_1 and L_2 of (9) used for fabrication now become:

$$L_1 = 1\text{nH and } L_2 = 3.6\text{nH}$$

The coupler circuit was fabricated on a substrate from Roger Duroid [21], with $\varepsilon_r = 3.4$ and the 0.305 mm thickness. The comparison of the magnitude and phase of the transmission coefficients and losses as functions of the DC biasing diode voltage is shown in Fig. 5 and Fig. 6 respectively. Frequency dependency of the transmission coefficients
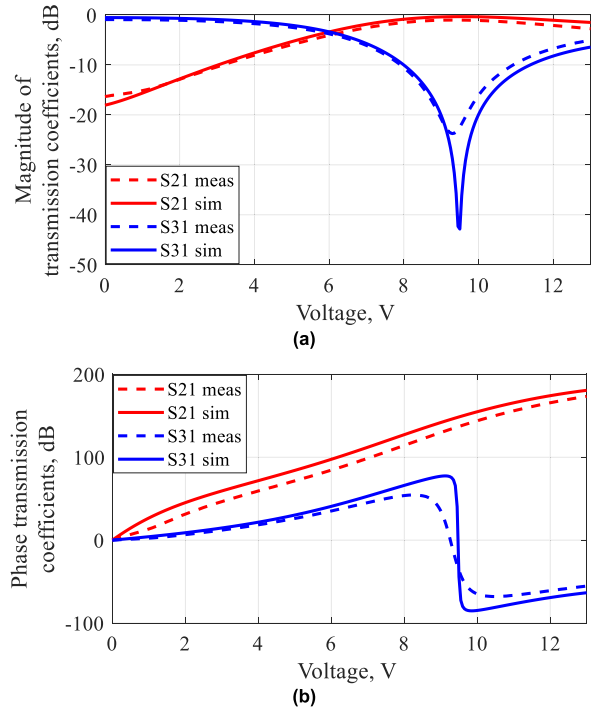

FIGURE 5. Measured and simulated magnitude (a) and phase (b) of the transmission coefficients of proposed coupler as function of bias voltage at 2.5 GHz.
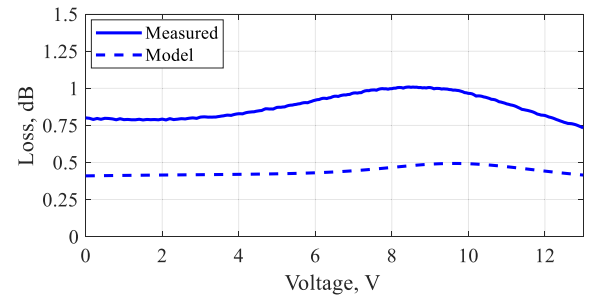

FIGURE 6. Measured and simulated loss of proposed coupler as function of DC bias voltage at 2.5 GHz.

for different diodes DC bias voltages is shown on Fig. 7. For the given capacitance ratio, the power division ratio varies between -16 dB to 24 dB (dynamic range of 40 dB), which allows realizations of a wide range of different amplitude distributions. Losses, as reported in Fig. 6, are defined as the reciprocal sum of the power transmission coefficients for both output ports:

$$Loss = 10\log_{10}\left(\frac{1}{|S_{21}|^2 + |S_{31}|^2}\right) \quad (10)$$

where S_{21} and S_{31} are the transmission coefficients from port 1 to ports 2 and 3, correspondingly. Insertion losses measured across the applied DC bias voltages from 1 to 13 V do not exceed 1 dB.

III. BEAMFORMING NETWORK
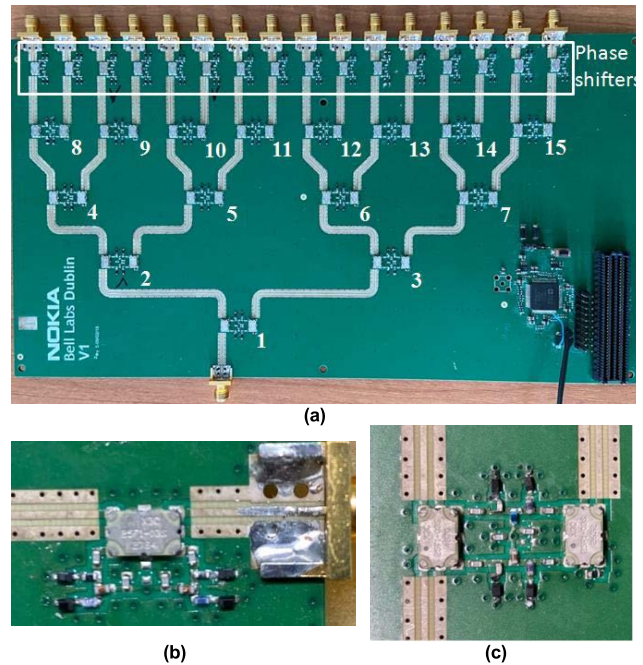### A. HARDWARE AND EXPERIMENTAL SETUP
To demonstrate the attractive features of the proposed variable coupler, a PCB-based beamforming network with
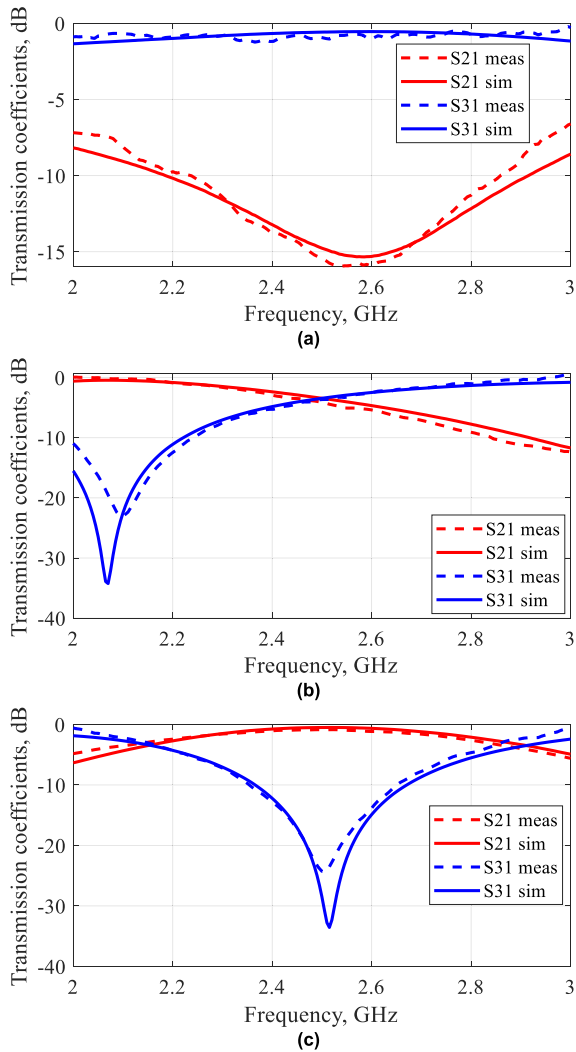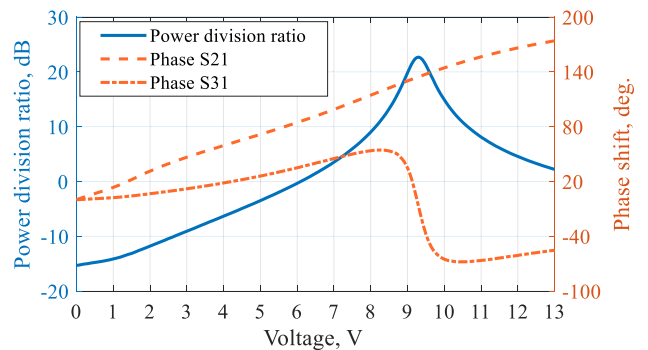
FIGURE 7. Measured and simulated transmission coefficients of the coupler as a function of frequency for next diodes DC bias voltages: 0 V (a), 6 V (b), 9.5 V (c).

FIGURE 8. Manufactured PCB-based beamforming network with numbered couplers (a), single phase shifter (b), single coupler (c).

FIGURE 9. Power division ratio and normalized phase of the transmission coefficients as function of applied DC bias voltage.

16 outputs has been designed, simulated and fabricated, Fig. 8. At this point, it needs to be mentioned that general n x m antenna beamforming realizations are also possible, however, that is likely to require multi-layered substrates in order to feed individual antenna elements with signals of correct magnitudes and phases.

For the present 1×16 realization, the dielectric substrate for the RF layer, RO4003C from Rogers [21] with $\varepsilon_r = 3.4$ and the 0.305 mm thickness was used. For DC biasing and signaling, the R-1533 laminate from Panasonic [22] with a thickness of 0.203 mm was used. Dimensions of the designed board are 275×150 mm ($2.3\lambda \times 1.25\lambda$ at 2.5 GHz). The circuit consists of 15 couplers providing the required power division among all output ports and 16 phase shifters to provide independent phase shifts for each output path. Phase shifters and couplers are controlled by the Digital-to-Analog-Converter (DAC) AD5371 from Analog Devices [19] through individual bias lines placed in the signaling layer. The

couplers and phase shifters were characterized and designed to operate at a DC bias voltage range from 0 V to 13 V, since this is the maximum achievable unipolar voltage range obtained by the chosen DAC, as mentioned previously. The power division ratios, as well as phases of the transmission coefficients were characterized as a function of applied bias voltage, Fig. 9.

As can be seen from this graph the dynamic range is around 40 dB, achieved by varying the DC bias voltage in the range from 0 to 9.3 V. The asymmetrical power division ratio evident from this figure is caused by the additional reactance introduced by the transmission line between the two resonant circuits formed using the varactor diodes and inductors L_1 and L_2. In addition, the DC biasing circuit is connected at the midpoint of the transmission line, Fig. 8 (b), which further disrupts the symmetry of the proposed variable coupler.
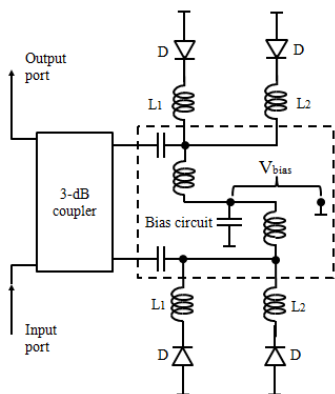
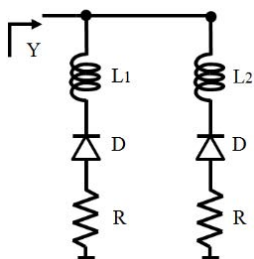**FIGURE 10. Equivalent circuit of the phase shifter.**

FIGURE 11. Ideal resonance load for phase shifter with parasitic resistance R.

Furthermore, due to the losses in the resonant circuits, the phase difference between the transmitted and reflected signals is not 90^0 as predicted by (5) and (6), but it exhibits a slope which is a function of the applied DC bias voltage, Fig. 9. If necessary, additional phase compensation circuits can be added so as to ensure the ideal 90° phase difference between the two output ports.

The phase shifter has a similar structure as the variable coupler. However, it consists of only one 3-dB, 90° coupler, and two resonant circuits with varactor diodes that allow the achievement of maximum phase shift, as shown in Fig. 10. The values of the inductors, L_1 and L_2 are the same as in the case of the coupler. The range of the applied DC bias voltage is also the same as in the case of the variable coupler, from 0 to 13 V.

The phase shifter of Fig. 10 was also characterized theoretically and experimentally. In order to theoretically assess the performance of the phase shifter, the circuit of Fig. 11 is used. Here, losses are represented by resistor R. The admittance of this circuit for the case when the parasitic resistance is zero ($R = 0$) can be written as:

$$Y = -j\frac{(C_v - C_{vmax})\,\omega C_v C_{vmin} + (C_v - C_{vmin})\,\omega C_v C_{vmax}}{(C_v - C_{vmax}) + (C_v - C_{vmin})}$$

(11)

Here, it was assumed that the values of the inductors are chosen in accordance with (9). The condition for the parallel
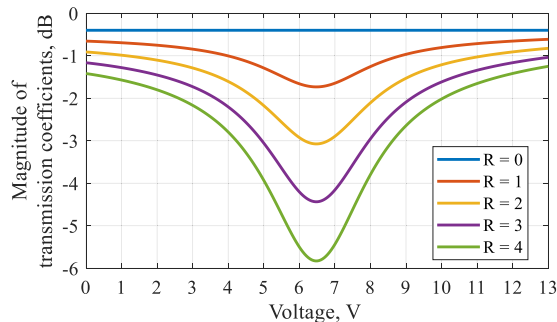

FIGURE 12. Reflection coefficient for ideal phase shifter as a function of voltage for different values of parasitic resistance R.

resonance ($Y = 0$) is achieved when:

$$C_v = 2\frac{C_{vmax}C_{vmin}}{C_{vmax} + C_{vmin}}$$

(12)

For cases when the parasitics (varactor diode, inductors, PCB losses) cannot be ignored, the admittance, Y, for the values of C_v given by (12) is no longer zero but attains finite, non-zero, real values. The voltage dependence of C_v of (12) is inferred from the knowledge of the dependence of the junction capacitance as a function of the DC bias voltage, given by:

$$C(V) = C_0 \left(1 + \frac{V}{V_i}\right)^{-M}$$

(13)

where C_0 is the capacitance at 0 V, M is the grading coefficient and V_i is the junction potential. For the present diode, $C_0 = 23$ pF, $V_i = 0.55$ V, $M = 1.15$. Combining (12) and (13) one arrives at the DC bias voltage at which the parallel resonance is reached:

$$V = V_i \left[\frac{C_0(C_{vmin} + C_{vmax})}{2C_{vmin}C_{vmax}}\right]^{\frac{1}{M}} - V_i$$

(14)

Having obtained the dependence of the admittance of the reflective loads as a function of the DC bias voltage, it is now possible to compute, through simulations, the performance of a phase shifter as a function of applied DC bias voltage, Fig. 12 and for different values of parasitic resistance R at the design frequency of 2.5 GHz. In the present phase shifter, parasitics represented by R are equal to the sum of the resistances of the varactor diode, ($R_d = 2.4\Omega$) and a series inductor $R_L = 0.5$ Ω, yielding a composite parasitic resistance of $R = 2.9$ Ω. The losses of a 3-dB coupler, based on the manufacturer's datasheet are 0.2 dB. To this end, the values of inductors L_1 and L_2 are calculated using (9). It can be seen that the parasitics play a crucial role on the performance of the proposed phase shifter. This is particularly obvious at a bias voltage of 6.5 V, which corresponds to the position of the parallel resonance, as elaborated earlier.

Fig. 13 shows the measured and simulated phase shift and magnitude of the transmission coefficient as a function of the applied DC bias voltage. A comparison of the simulated and measured performance of the present phase shifter reveals
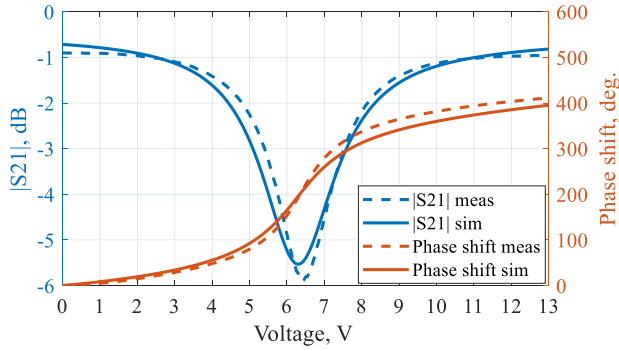
FIGURE 13. Measured and simulated phase shift and magnitude of the transmission coefficient as a function of applied bias voltage at 2.5 GHz.
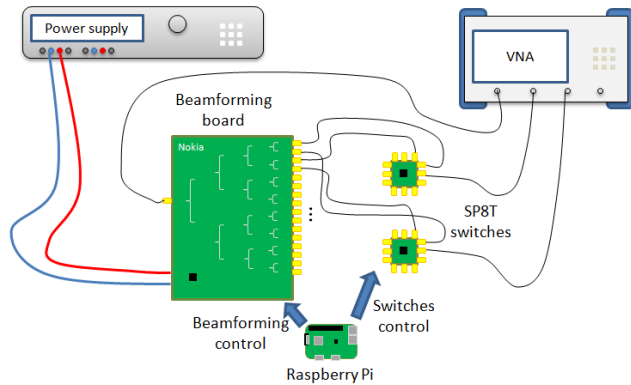

FIGURE 14. Measurement setup of the beamforming board.

an excellent agreement. The maximum predicted insertion loss occurs as 6.5 V for both the simulated and measured cases, however, the measured insertion loss is approximately 0.4 dB greater, possibly due to the unaccounted for sources of loss (manufacturing tolerances, bias circuit losses and losses in plated vias). The measured insertion loss stands at 5.9 dB, whereas the simulated insertion loss stands at 5.5 dB. The maximum shift obtained from the measured phase shifter stands at 420°, whereas the maximum phase shift of its simulated counterpart is approximately 400°.

Having explained the design and performances of the variable couplers and phase shifters in detail, it is now pertinent to describe the measurement set-up needed for the measurement of the beam-forming board of Fig. 8. To measure the transmission coefficients between port 1 and all 16 output ports on the complete beamforming board of Fig. 8, Single-Pole-8-Throw (SP8T) Analog Devices RF switches were used, Fig. 14, [19]. The Raspberry Pi 4 platform [23], driven by Matlab [24] was used to control the operating voltages on the DAC outputs via the Serial Peripheral Interface (SPI) interface, as well as the SP8T RF switches. The linear performance of the board was measured using the R&S ZNB20 Vector Network Analyzer, and the R&S HMP4030 power supply. To exclude the influence of the SP8T switches on the performance of the beamforming network, their characteristics were measured separately and adequately taken into account.

B. CURRENT DISTRIBUTION OPTIMIZATION

To provide an arbitrary distribution of magnitudes and phases of the transmission coefficients along the output ports of the board, it is required to independently control 31 DC bias voltages for each coupler and phase shifter. The problem is further exacerbated due to the fact that phases of the signals at the output of the couplers are dependent on the split ratio (Fig. 9), and that the magnitudes of the transmission coefficient of phase shifters are dependent on their phase delay (Fig. 13). In other words, it is not possible to independently control magnitudes and phases. As such, due to the complex nature of control, it was decided to use an optimization procedure to determine the required DC bias voltages for variable couplers and phase shifters. For this purpose, the following analytical model describing the beamforming circuit was developed:

$$
\begin{pmatrix} S_{1,1} \\ S_{2,1} \\ \cdots \\ S_{15,1} \\ S_{16,1} \end{pmatrix} = \begin{pmatrix} PS_1 & 0 & \cdots & 0 & 0 \\ 0 & PS_2 & & 0 & 0 \\ \vdots & & \ddots & & \vdots \\ 0 & 0 & & PS_{15} & 0 \\ 0 & 0 & \cdots & 0 & PS_{16} \end{pmatrix}
$$

$$
\times \begin{pmatrix} PD_8 \begin{bmatrix} 0 \\ 0 \end{bmatrix} & \cdots & \begin{bmatrix} 0 \\ 0 \end{bmatrix} \begin{bmatrix} 0 \\ 0 \end{bmatrix} \\ \begin{bmatrix} 0 \\ 0 \end{bmatrix} PD_9 & & \begin{bmatrix} 0 \\ 0 \end{bmatrix} \begin{bmatrix} 0 \\ 0 \end{bmatrix} \\ \vdots & \ddots & \vdots \\ \begin{bmatrix} 0 \\ 0 \end{bmatrix} \begin{bmatrix} 0 \\ 0 \end{bmatrix} & PD_{14} \begin{bmatrix} 0 \\ 0 \end{bmatrix} \\ \begin{bmatrix} 0 \\ 0 \end{bmatrix} \begin{bmatrix} 0 \\ 0 \end{bmatrix} & \begin{bmatrix} 0 \\ 0 \end{bmatrix} PD_{15} \end{pmatrix}
$$

$$
\times \begin{pmatrix} PD_4 \begin{bmatrix} 0 \\ 0 \end{bmatrix} & \begin{bmatrix} 0 \\ 0 \end{bmatrix} \begin{bmatrix} 0 \\ 0 \end{bmatrix} \\ \begin{bmatrix} 0 \\ 0 \end{bmatrix} PD_5 & \begin{bmatrix} 0 \\ 0 \end{bmatrix} \begin{bmatrix} 0 \\ 0 \end{bmatrix} \\ \begin{bmatrix} 0 \\ 0 \end{bmatrix} \begin{bmatrix} 0 \\ 0 \end{bmatrix} & PD_6 \begin{bmatrix} 0 \\ 0 \end{bmatrix} \\ \begin{bmatrix} 0 \\ 0 \end{bmatrix} \begin{bmatrix} 0 \\ 0 \end{bmatrix} & \begin{bmatrix} 0 \\ 0 \end{bmatrix} PD_7 \end{pmatrix}
$$

$$
\times \begin{pmatrix} PD_2 \begin{bmatrix} 0 \\ 0 \end{bmatrix} \\ \begin{bmatrix} 0 \\ 0 \end{bmatrix} PD_3 \end{pmatrix} \times PD_1 \qquad (15)
$$

where $S_{n,1}$ is the complex transmission coefficient between the input and n-th output ports, PS_n is the complex transmission coefficient of the n-th phase shifter, where n is the output port index ($n = 1\ldots N$), and PD_p is a power division matrix, which consists of two transmission coefficients between the input and output ports of the p-th coupler ($p = 1\ldots N$-1), where N stands for the number of output ports. Transmission coefficients of couplers and the phase shifters are functions of the applied DC bias voltages. Since it is impossible to directly measure the performance of individual couplers and phase shifters on the assembled board, we assume that the

characteristics of all couplers and phase shifters given by (15) are identical.

Optimization was performed with the following goal function:

$$G(V) = \sqrt{\frac{\sum_{n=1}^{N}\left(\left|S_{n,1}(V)\right| - |I_n|\right)^2}{N-1}}$$

$$+ \sqrt{\frac{\sum_{n=1}^{N}\left(angle\left(S_{n,1}(V)\right) - angle(I_n)\right)^2}{N-1}} \quad (16)$$

where I_n is the required complex current distribution along the board output ports, which is numerically identical to transmission coefficients $S_{n,1}$ from (15), and V is a vector of DC bias voltages. Minimization of this goal function was done by the pattern search method [25]. As a result of the optimization, the DC bias voltage value for every coupler and phase shifter is found; they were subsequently used in measurements.

C. BOARD CHARACTERIZATION

In order to estimate the losses of the proposed beamforming network of Fig. 8, the optimization procedure of the previous section was used to yield the DC bias voltages needed to be applied to the couplers and phase shifters necessary to obtain uniform distribution of both the magnitudes and phases at the 16 output ports of the beamforming network.

Fig. 15 provides a comparison among the measured, optimized and ideal results needed to obtain a uniform distribution of magnitudes and phases. It can be seen from Fig. 15 (a) that the estimated model losses are just over 6 dB, while measured losses are about 8 dB with the magnitude of error of about ±1.5 dB. The total losses in both simulated and measured cases are composed of losses due to the variable couplers (input signal transverses 4 variable couplers), a phase shifter and transmission lines. Measured losses exhibit an additional 2 dB loss compared to the model due to unaccounted losses in transmission lines, connectors and soldering. The variation of losses of about ±1.5 dB is due to the possibility that the individual variable couplers and phase shifters may not exhibit the same performance. The phase error is about ±10°, Fig. 15 (b), which is admissible for beamsteering applications and corresponds to an error equivalent to a 5-bit phase shifter. It could possibly be related to the fact that not all variable couplers and phase shifters are identical, inferring differences in the performance.

Fig 16 shows the optimization-obtained DC bias voltages for the couplers and phase shifters needed to obtain a uniform distribution of magnitudes and phases at the output. The DC bias voltages needed by the couplers, Fig. 16 (a), lie in the range of 5.75 V ±0.3 V, and this small deviation is attributed to the possibility that realized couplers may not be to fully identical and that there could exist certain differences among them. Here, one needs to be reminded that the output signal at each port transverses 4 variable couplers and one phase
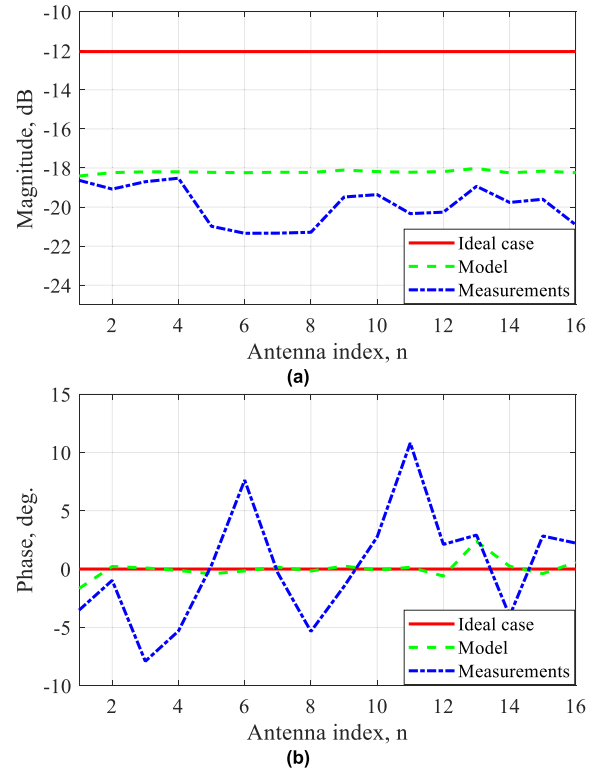

FIGURE 15. Ideal, optimized and measured results for uniform magnitude(a) and phase (b) distribution.
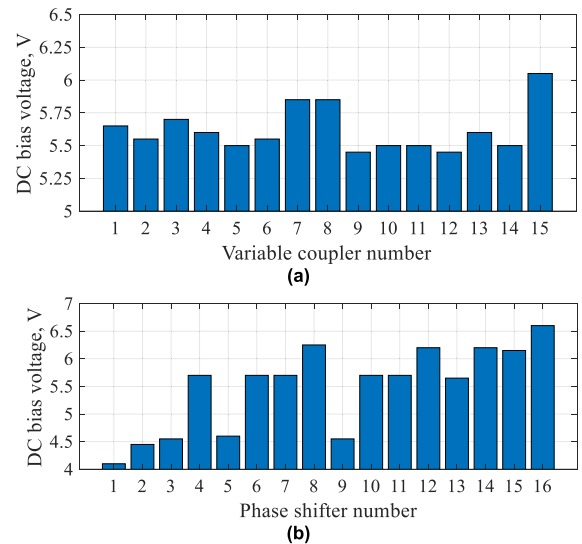

FIGURE 16. Voltages obtained for couplers (a) and phase shifters (b).

shifter and that small variations among them affect the entire signal path. Fig. 16 (b) shows the DC bias voltages required by the phase shifters in order achieve uniform distribution. The voltage range yielded by the optimization in this case lies between 4.1 V to 6.6 V or 5.35 V ±1.25 V, which is somewhat larger compared to the deviation of 0.3 V as experienced by the voltages need by the couplers. However, since there is only one phase shifter per output branch, such a phase

TABLE 1. Radiation pattern parameters.

Case	z_0	z_1	SLL, dB	Beam width, °
1	1.01	0.81	-13	6.8
2	1.01	0.69	-13	8
3	1.01	0.56	-13	10

shifter needs to account for any possible phase performance differences at the preceding sections containing the variable couplers.

IV. BEAMFORMING ANALYSIS

A. ARRAY SYNTHESIS

In this section, beam-reconfigurable capabilities of the considered beamforming network are analyzed. As a starting point, one needs to solve a direct problem of antenna arrays synthesis – to find the amplitude and phase excitation distributions along the given antenna array outputs providing the required amplitude radiation pattern $F_{ideal}(\theta)$.

Here, we analyze radiation patterns with a constant pre-defined sidelobe level (SLL) that requires simultaneous control of both amplitudes and phases of the excitation signals. This is used to highlight the features of the beamforming network based on the proposed variable couplers. The radiation patterns could be described with Chebyshev polynomials [26], [27]:

$$F_{ideal}(\theta) = T_N(\theta, \theta_0, z_0, z_1)$$

$$= \begin{cases} \cos\{Nacos[z_0\cos[z_1(u(\theta) - u(\theta_0))]]\}, \\ \quad if\ z_0\cos[z_1(u(\theta) - u(\theta_0))] \leq 1 \\ \cosh\{Nacosh[z_0\cos[z_1(u(\theta) - u(\theta_0))]]\}, \\ \quad if\ z_0\cos[z_1(u(\theta) - u(\theta_0))] > 1 \end{cases} \quad (17)$$

where $u(\theta) = (\pi d/\lambda)\sin(\theta)$, parameter z_1 defines the radiation pattern beamwidth, θ is the angle between $-\pi/2$ to $\pi/2$, and parameter z_0 is the scale factor, which specifies the SLL with respect to the main beam maximum [26]:

$$\xi(z_0) = -20\log(T_N(0, 0, z_0, z_1)) \quad (18)$$

After that, for the given amplitude radiation pattern $F_{ideal}(\theta)$, the complex values of antenna element excitation currents I_n can be calculated using (19) [28]:

$$I_n = \frac{1}{2\pi}\int_{-\frac{\pi}{2}}^{\frac{\pi}{2}} F_{ideal}(\theta)\cos(\theta)\,e^{(-jkdn\sin(\theta))}d\theta \quad (19)$$

where n is the antenna element index.

For a given SLL and different beam widths, given in Table 1, the required complex current distributions along the output ports of the board of Fig. 8, using (17) and (19) are calculated. The obtained magnitudes of I_n are shown in Fig. 17 (a) (solid lines). It should be noted that the values I_n are normalized in a way that $\sum|I_n|^2 = 1$, which corresponds to ideal lossless re-distribution of the input power among the output ports of the beamforming network.
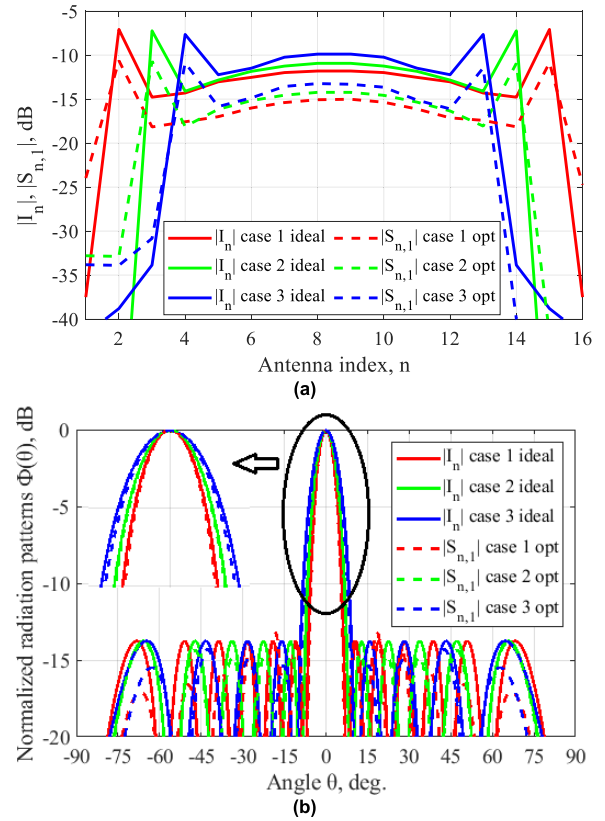

FIGURE 17. Ideal I_n and optimized $S_{n,1}$ results for normalized magnitude distribution (a) and radiation pattern (b).

Using the optimization procedure described in Section III B, the calculated ideal current distribution I_n applied to the goal function (16) allows one to infer DC bias voltages needed for each coupler and phase shifter, which provide an optimum complex current distribution $S_{n,1}$ for the analyzed beamforming settings. The obtained magnitudes of $S_{n,1}$ corresponding to different cases described in Table 1, are presented in Fig. 17 (a) (dashed lines). As one can see, most power is distributed among the ports in the middle of the beamforming network, while the number of "unused" peripheral ports increases as a function of increased beamwidth. The observed discrepancy between the ideal and optimized magnitude and phase distributions is very small and could be explained by insufficient optimization accuracy and losses.

Based on the complex excitation distribution along the output ports, a radiation pattern of a 16-element linear antenna array, assuming that isotropic radiators with $\lambda/2$ spacing are used instead of real antenna elements, (so called *Array Factor*) [29] can be calculated using:

$$F(\theta) = \sum_{n=1}^{N} I_n e^{j\pi(n\sin\theta)} \quad (20)$$

where N represents the number of output ports (in this study $N = 16$) and I_n is the complex current distribution along the output ports of the board as obtained from (19), as explained earlier. To calculate the optimized radiation patterns I_n should
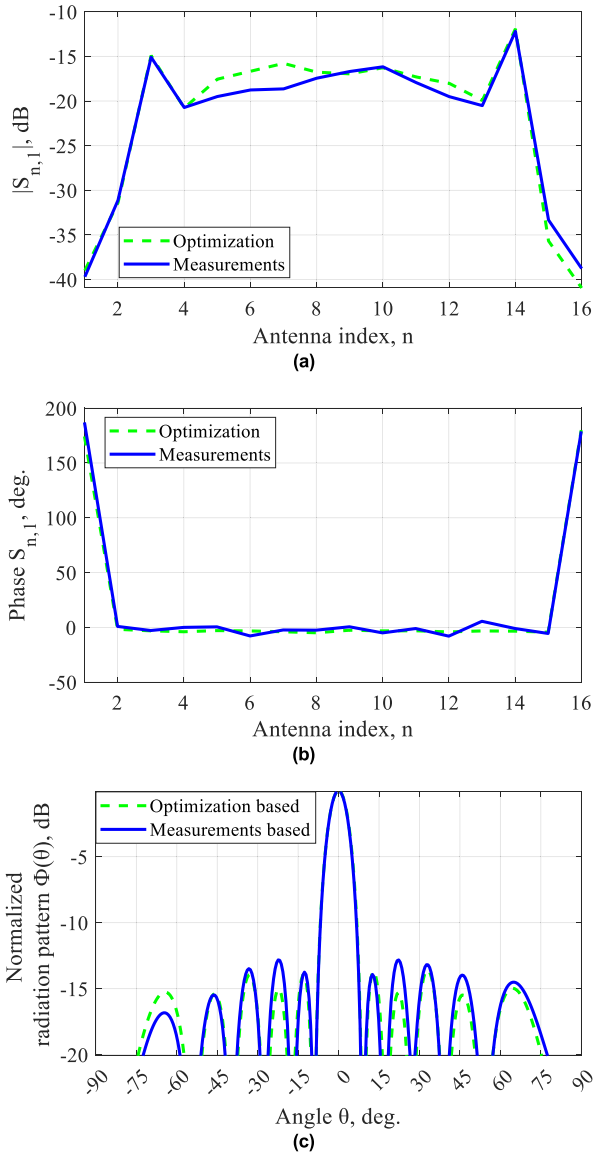
FIGURE 18. Optimized and measured results for magnitude distribution (a), phase distribution (b) and radiation pattern (c) for the case of 8° beamwidth and SLL of −13 dB.

be replaced by transmission coefficients $S_{n,1}$ from (16). The analysis of the obtained ideal (solid lines) and optimized (dashed lines) normalized radiation patterns $\hat{O}(\theta)$ (21), shows that the SLL does not exceed the pre-determined level of −13 dB, Fig. 17 (b).

$$\Phi(\theta) = -20 \cdot \log\left[\frac{F(\theta)}{\max(F(\theta))}\right] \quad (21)$$

These results prove that the proposed beamforming network design is capable of an arbitrary division of power between all output ports of an antenna array.

B. MEASUREMENTS RESULTS
As was mentioned before, the developed optimization procedure allows one to find optimum DC bias voltages necessary to be applied to variable couplers and phase shifters,
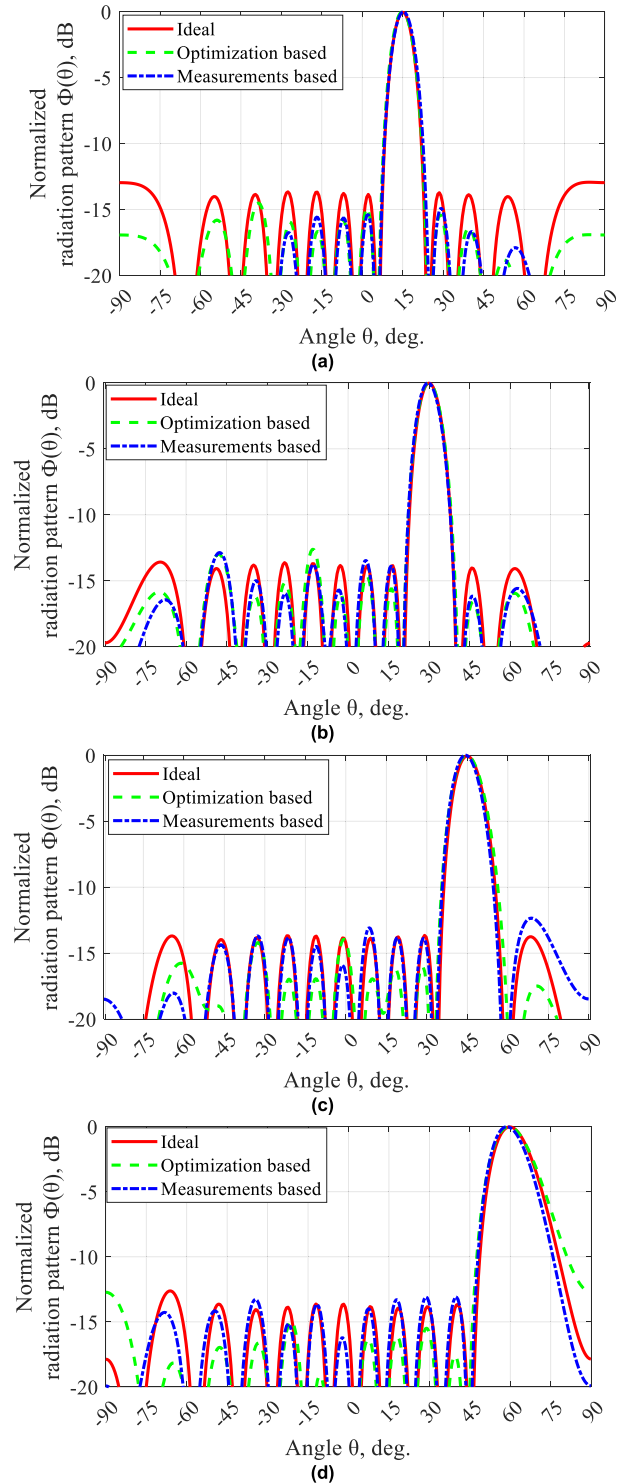
FIGURE 19. Ideal, optimized and measured results of normalized radiation pattern for 15° (a), 30° (b), 45° (c) and 60° (d) scan angles.

Fig. 8. By applying the DC bias voltages obtained using the optimization procedure for a scenario pertaining to the 8° beamwidth and SLL of −13 dB (case 2 from Table 1), the complex transmission coefficients $S_{n,1}$ between the board input and 16 output ports were measured at a frequency of

2.5 GHz. The measured magnitudes and phases of $S_{n,1}$ are shown in Fig. 18 (a, b) (solid lines) along with previously optimized values (dashed lines). Based on the measured transmission coefficients, the normalized radiation pattern was calculated using (20) - (21) and shown in Fig. 18 (c). After that, the beam steering capabilities of the designed network were investigated. For this purpose, the above-described optimization procedure and measurements of complex transmission coefficients $S_{n,1}$ were repeated for scenarios corresponding to 15°, 30°, 45° and 60° main beam directions. The radiation patterns based on optimized and measured transmission coefficients $S_{n,1}$ are presented in Fig. 19 along with ideal radiation patterns.

As one can see, the measurement-based radiation patterns are in a good agreement with the theoretically predicted radiation patterns around the main lobe, inferring that the proposed beamforming network supports beam scanning within the range from -60° to +60°. In turn, the observed SLL differences among the optimized and measured radiation patterns, which for some cases can be more than 5 dB, Fig. 19 (a), can be primarily explained by the variation among the characteristics of different couplers and phase shifters, as well as the additional losses in the transmission lines, connectors and soldered joints that were not possible to be taken into account during the optimization routine.

V. CONCLUSION

In this paper a new beamforming network for a given number of antenna elements is presented. The proposed architecture, based on a novel design of the continuously variable coupler, theoretically capable of an arbitrary division of power between its two output ports, is introduced. The control of power division was achieved by means of varactor diodes capable of modulating its reactance with varying DC bias voltage.

To adequately control the beamforming network capabilities of the proposed network, an optimization procedure was used for the determination of exact DC bias voltages needed to be applied to the couplers and phase shifters, allowing one to gain maximum possible advantage of the proposed network by enabling the creation of arbitrary current distributions on all antenna elements.

As an example of the usability of the proposed concept, a prototype of the proposed beamforming network for a 16-element linear antenna array has been fabricated and measured at 2.5 GHz. Excellent agreement between theoretical and measured radiation patterns for 0°, 15°, 30°, 45° and 60° main beam directions was obtained, verifying the beamforming capabilities of the proposed network and the developed optimization procedure. Our future work centers on the integration of the proposed beamforming network and a real antenna array in order to stipulate the benefits of the presented solution. In addition, the proposed beamforming network is particularly suitable for implementation of directional modulation due to the necessity to provide unique magnitude

distributions for different modulation symbols. This will also form part of our future work.

REFERENCES

[1] (2022). *A Research Outlook Towards 6G*. [Online]. Available: https://www.ericsson.com/en/reports-and-papers/white-papers/a-research-outlook-towards-6g
[2] S. Ghosh and D. Sen, "An inclusive survey on array antenna design for millimeter-wave communications," *IEEE Access*, vol. 7, pp. 83137–83161, 2019.
[3] A. H. Naqvi and S. Lim, "Review of recent phased arrays for millimeter-wave wireless communication," *Sensors*, vol. 18, no. 10, p. 3194, 2018.
[4] M. Norooziarab, D. McCloskey, D. S. Kozlov, V. V. Kirillov, S. Bulja, F. Pivit, and P. Rulikowski, "Millimeter-wave 3D printed Luneburg lens antenna," in *Proc. IEEE Radio Antenna Days Indian Ocean (RADIO)*, Sep. 2019, pp. 1–2.
[5] Y. Amarasinghe, R. Mendis, R. Shrestha, H. Guerboukha, J. Taiber, M. Koch, and D. M. Mittleman, "Broadband wide-angle terahertz antenna based on the application of transformation optics to a Luneburg lens," *Sci. Rep.*, vol. 11, no. 1, pp. 1–8, Dec. 2021.
[6] P. Turalchuk, I. Munina, P. Kapitanova, D. Kholodnyak, D. Stoepel, S. Humbla, J. Mueller, M. A. Hein, and I. Vendik, "Broadband small-size LTCC directional couplers," in *Proc. 40th Eur. Microw. Conf.*, Sep. 2010, pp. 1162–1165.
[7] V. Palazzi, F. Alimenti, P. Mezzanotte, and L. Roselli, "Novel magnitude and phase reconfigurable 1 × 4 RF power distribution network," *IEEE Trans. Microw. Theory Techn.*, vol. 69, no. 1, pp. 29–42, Jan. 2021.
[8] S. Oh, J. J. Koo, M. S. Hwang, C. Park, Y. J. Jeong, J. S. Lim, K. S. Choi, and D. Ahn, "An unequal Wilkinson power divider with variable dividing ratio," in *IEEE MTT-S Int. Microw. Symp. Dig.*, Jun. 2007, pp. 411–414.
[9] H. Fan, X. Liang, J. Geng, R. Jin, and X. Zhou, "Reconfigurable unequal power divider with a high dividing ratio," *IEEE Microw. Wireless Compon. Lett.*, vol. 25, no. 8, pp. 514–516, Aug. 2015.
[10] H. Fan, J. Geng, X. Liang, R. Jin, and X. Zhou, "A three-way reconfigurable power divider/combiner," *IEEE Trans. Microw. Theory Techn.*, vol. 63, no. 3, pp. 986–998, Mar. 2015.
[11] L. Guo, H. Zhu, and A. M. Abbosh, "Wideband tunable in-phase power divider using three-line coupled structure," *IEEE Microw. Wireless Compon. Lett.*, vol. 26, no. 6, pp. 404–406, Jun. 2016.
[12] A. Abbosh and L. Guo, "Three-way signal divider with tunable ratio for adaptive transmitting arrays," *IET Microw., Antennas Propag.*, vol. 6, no. 12, pp. 1318–1324, 2012.
[13] K.-K.-M. Cheng and S. Yeung, "A novel rat-race coupler with tunable power dividing ratio, ideal port isolation, and return loss performance," *IEEE Trans. Microw. Theory Techn.*, vol. 61, no. 1, pp. 55–60, Jan. 2013.
[14] K.-K. M. Cheng and M.-C. J. Chik, "A frequency-compensated rat-race coupler with wide bandwidth and tunable power dividing ratio," *IEEE Trans. Microw. Theory Techn.*, vol. 61, no. 8, pp. 2841–2847, Aug. 2013.
[15] S. Bulja and A. Grebennikov, "A novel variable power divider with continuous power division," *Microw. Opt. Technol. Lett.*, vol. 55, no. 7, pp. 1684–1686, Apr. 2013.
[16] S. Bulja, S. Kucera, and V. Venkateswaran, "An adaptive antenna array and an apparatus and method for feeding signals to an adaptive antenna array," European Patent 3 128 612 A1, Aug. 4, 2015.
[17] TTM Technologies. (2022). [Online]. Available: https://www.ttm.com
[18] Macom. (2021). [Online]. Available: https://www.macom.com
[19] Analog Devices. (2022). [Online]. Available: https://www.analog.com
[20] Murata. (2022). [Online]. Available: https://www.murata.com
[21] Rogers Corporation. (2022). [Online]. Available: https://www.rogerscorp.com/
[22] Panasonic. (2022). [Online]. Available: https://industrial.panasonic.com
[23] Raspberry Pi Foundation. (2022). [Online]. Available: https://www.raspberrypi.org
[24] MathWorks. (2022). [Online]. Available: https://www.mathworks.com
[25] C. Audet and J. E. Dennis, Jr., "Analysis of generalized pattern searches," *SIAM J. Optim.*, vol. 13, no. 3, pp. 889–903, Feb. 2002.

[26] C. L. Dolph, "A current distribution for broadside arrays which optimizes the relationship between beam width and side-lobe level," *Proc. IRE*, vol. 34, no. 6, pp. 335–348, Jun. 1946.

[27] O. G. Vendik and D. S. Kozlov, "Phased antenna array with a sidelobe cancellation for suppression of jamming," *IEEE Antennas Wireless Propag. Lett.*, vol. 11, pp. 648–650, 2012.

[28] R. J. Mailloux, *Phased Array Antenna Handbook*. Boston, MA, USA: Artech House, 1994.

[29] C. A. Balanis, *Antenna Theory: Analysis and Design*. Hoboken, NJ, USA: Wiley, 2015.

VITALY KIRILLOV (Student Member, IEEE) received the B.Sc. and M.Sc. degrees in radio engineering from Saint Petersburg Electrotechnical University LETI, St. Petersburg, Russia, in 2016 and 2018, respectively, where he is currently pursuing the Ph.D. degree. In 2019, he had a six-month internship with Nokia Bell Labs, Dublin, Ireland. From 2021 to 2022, he was a Visiting Research Student at Queen's University Belfast. His primary research interests include passive and active devices for microwave and mm-wave frequency ranges. The research area is mostly focused on transmitarray and reflectarray structures for communication applications.

DMITRY KOZLOV received the B.Sc. and M.Sc. degrees in radiophysics from Saint Petersburg Electrotechnical University LETI, St. Petersburg, Russia, in 2009 and 2011, respectively, and the Ph.D. degree in electronics and electrical engineering from Queen's University Belfast (QUB), Belfast, U.K., in 2016. He was a Marie Curie Early-Stage Researcher with the Institute of Electronics, Communications and Information Technology, QUB, from 2013 to 2016. He is currently with Nokia Mobile Networks, Ulm, Germany. His research interest includes microwave and antenna theory, including synthesis of antenna arrays, and analysis of nonlinear distortions in microwave passive and active devices.

PAWEL RULIKOWSKI (Member, IEEE) received the Ph.D. degree from the Cork Institute of Technology (CIT), Cork, Ireland, in 2011. From 2002 to 2012, he was with the NIMBUS Centre for Embedded Systems Research, CIT. From 2013 to 2020, he has been a member of Technical Staff with Nokia Bell Labs (formerly Alcatel-Lucent Bell Labs), Dublin, Ireland. From 2020 to 2021, he was with Alpha Wireless, Ireland, where he was a RF Senior Design Engineer responsible for design and proof-of-concept builds of base station antennas. He has been involved in a variety of research and development projects with Irish and international industry in the areas of radio communication and microwave (MW) design for more than a decade. His current research interests include large-scale antenna systems (massive MIMO), RF/MW filter design, and novel materials applicable to high-frequency components.

SENAD BULJA (Senior Member, IEEE) received the B.Eng. (Hons.) and Ph.D. degrees from the University of Essex, Colchester, U.K., in 2002 and 2007, respectively.

From 2007 to 2010, he was a Senior Research Officer with the School of Computer Science and Electronic Engineering, University of Essex, where he led the characterization effort of liquid crystals at microwave and millimeter-wave frequencies, and the development of liquid-crystal-based millimeter-wave devices. He is currently a Principal Scientist at the Tyndall National Institute, in charge of creating a Radio Frequency (RF) Hardware Research Team. Previously, from 2010 to 2020, he was with Nokia Bell Labs, where he was a Senior Research Scientist. There, he led the research effort in the research and development of low-profile resonators and filters and the discovery of dielectric tunability of inorganic electro-chromic materials and RF switching capability of transition metal oxides. He is also the CTO and the Founder of a Nokia spin-out, ArqKos, which focuses on high-RF performance filters. He has authored/coauthored over 70 papers in international journals and conference proceedings and holds over 70 patents in the area of electromagnetics and wireless telecommunications. His current research interests encompass new tunable RF dielectric and optical media, RF filters, RF amplifiers, specialized antennas, complete RF transceivers, and a plethora of RF passive and active devices (attenuators, couplers, and phase shifters) up to 300 GHz.

Dr. Bulja is a fellow of the IET. He was a recipient of many awards, such as the Award for being Nokia's Top Inventor and the Best Innovation Prize from the European Space Agency.

● ● ●